Research Paper

Link between SARS-CoV-2 emissions and airborne concentrations: Closing the gap in understanding

G. Buonanno [a,b,e], A. Robotto [c,e], E. Brizio [c,e], L. Morawska [b,e], A. Civra [d,e], F. Corino [c,e], D. Lembo [d,e], G. Ficco [a,e], L. Stabile [a,e,*]

[a] Department of Civil and Mechanical Engineering, University of Cassino and Southern Lazio, Cassino, FR, Italy
[b] International Laboratory for Air Quality and Health, Queensland University of Technology, Brisbane, Qld, Australia
[c] Environmental Protection Agency of Piedmont (ARPA Piemonte), Italy
[d] Dept. of Clinical and Biological Science, Azienda Ospedaliero-Universitaria San Luigi Gonzaga, University of Turin, Italy
[e] Infectious Diseases Unit, Department of Medical Sciences, Amedeo di Savoia Hospital, University of Turin, Torino, Italy

HIGHLIGHTS

- The airborne transmission of SARS-CoV-2 remains surprisingly controversial.
- A direct proof of SARS-CoV-2 airborne transmission is still required.
- The link between emission and airborne concentration is experimentally demonstrated.
- A theoretical approach estimating SARS-CoV-2 airborne concentrations is validated.
- The measurement of airborne SARS-CoV-2 concentration presents high uncertainties.

GRAPHICAL ABSTRACT
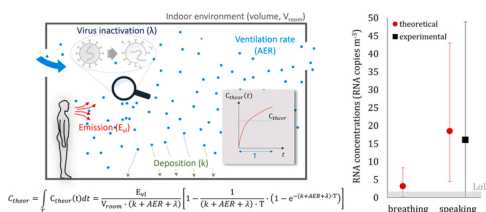
ARTICLE INFO

Editor: Dr. Danmeng Shuai

ABSTRACT

The airborne transmission of SARS-CoV-2 remains surprisingly controversial; indeed, health and regulatory authorities still require direct proof of this mode of transmission. To close this gap, we measured the viral load of SARS-CoV-2 of an infected subject in a hospital room (through an oral and nasopharyngeal swab), as well as the airborne SARS-CoV-2 concentration in the room resulting from the person breathing and speaking. Moreover, we simulated the same scenarios to estimate the concentration of RNA copies in the air through a novel theoretical approach and conducted a comparative analysis between experimental and theoretical results. Results showed that for an infected subject's viral load ranging between 2.4×10^6 and 5.5×10^6 RNA copies mL^{-1}, the corresponding airborne SARS-CoV-2 concentration was below the minimum detection threshold when the person was breathing, and 16.1 (expanded uncertainty of 32.8) RNA copies m^{-3} when speaking. The application of the predictive approach provided concentrations metrologically compatible with the available experimental data (i. e. for speaking activity). Thus, the study presented significant evidence to close the gap in understanding airborne transmission, given that the airborne SARS-CoV-2 concentration was shown to be directly related to the

SARS-CoV-2 emitted. Moreover, the theoretical analysis was shown to be able to quantitatively link the airborne concentration to the emission.

1. Introduction

The transmission mode of SARS-CoV-2 has divided experts and public health communities since the beginning of the COVID-19 pandemic. The main object of contention was the relevance of the airborne transmission route by inhalation of virus-laden respiratory particles emitted by an infected subject. In this context, the adoption of different terminology by scientific and medical communities, assigning different meanings to the terms "aerosol" and "droplets" (Randall et al., 2021), did not help. To avoid misinterpretation in the paper, we use the term "particles" rather than "aerosols" or "droplets". While interdisciplinary expert groups warned of the need to recognize the importance of the airborne transmission route (Greenhalgh et al., 2021; Morawska et al., 2020; Morawska and Cao, 2020), public health authorities were reluctant to accept this. In fact, the importance of airborne transmission was recognized by the World Health Organization (WHO), the US Centers for Disease Control and Prevention (CDC), and the Italian National Institute of Health (ISS) only after more than a year into the pandemic (WHO, 30 April 2021, www.who.int/news-room/questions-and-answers/item/coronavirus-disease-covid-19-how-is-it-transmitted; US CDC 7 May 2021, www.cdc.gov/coronavirus/2019-ncov/science/science-briefs/sars-cov-2-transmission.html, ISS 25 May 2021, Rapporto ISS COVID-19 n. 12/2021 available at www.iss.it/rapporti-covid-19). Indeed, public health authorities argued that to accept the relevance of airborne transmission, direct experimental evidence of its occurrence was needed. Interestingly, such verification has never been required for other transmission routes, such as droplet (larger particles) or fomite transmission (Greenhalgh et al., 2021).

1.1. Experimental evidence of COVID-19 airborne transmission

A large body of evidence was reported during the pandemic on different aspects of SARS-CoV-2 airborne transmission. First, SARS-CoV-2 was reported to remain viable in the air for up to 3 h, with a half-life of 1.1 h, in laboratory experiments (van Doremalen et al., 2020). In other field studies, viable SARS-CoV-2 was detected in air samples collected in hospital wards and rooms occupied by COVID-19 patients in the absence of aerosol-generating procedures (Lednicky et al., 2020; Liu et al., 2020; Santarpia et al., 2020; Stern et al., 2021). The hospital environment was the focus of these studies because of the certain presence of infected subjects; nonetheless, each of these studies used different methods. Lednicky et al. (2020) collected air samples in a hospital room in the presence of two COVID-19 patients through a gentle water vapor condensation method to address the question of whether viable SARS-CoV-2 can be found in airborne particles; the study recognized the presence of viable SARS-CoV-2 in air samples collected at different distances from the patients (2–4.8 m). Liu et al. Liu et al. (2020) measured the concentration of SARS-CoV-2 gene copies in airborne particles in different areas of two hospitals in Wuhan. They detected very low concentrations in well ventilated environments (e.g. isolation wards and ventilated patient rooms); however, where detected, viral RNA concentration showed peaks both in the sub-micrometer and super-micrometer particle ranges. Santarpia et al. (2020) collected air and surface samples to examine the viral shedding of 13 people with COVID-19 at the University of Nebraska Medical Center and detected viral contamination of all samples. They suggested that SARS-CoV-2 environmental contamination around COVID-19 patients is extensive

and hospital procedures must consider the risk of airborne transmission of the virus. Stern et al. (2021) collected air samples of three particle sizes in a hospital in Boston (Massachusetts, US): SARS-CoV-2 gene copies were present in 9% of the samples and in all size fractions at concentrations ranging from 5 to 51 RNA copies m^{-3}. Positive associations were found between the probability of a positive sample, the number of COVID-19 cases in the hospital, and the cases in Massachusetts. Nissen et al. (2020) took swab samples from individual ceiling ventilation openings and central ventilation filters in COVID-19 wards at Uppsala University Hospital, Sweden. The central ventilation HEPA exhaust filters from the ward detected evidence for the presence of the virus, showing that it can be transported over long distances and that airborne transmission of SARS-CoV-2 should be taken into consideration for preventive measures.

While all the reported studies investigated different aspects of potential COVID-19 airborne transmission, none of them provided a direct link between emissions from an infected subject and concentrations of viable SARS-CoV-2 in air as it would require designing an ad-hoc experimental campaign to measure simultaneously the SARS-CoV-2 viral load emission of an infected subject and the related airborne SARS-CoV-2 concentrations in controlled conditions. Such experiments are not available in the scientific literature; thus, the emission-to-airborne concentration direct link was still considered a missing aspect to prove beyond doubt the airborne transmissibility of COVID-19.

1.2. Aims

The aim of this study was to fill this experimental gap and provide the so-called "smoking gun". To this end we have performed an experimental analysis measuring SARS-CoV-2 RNA copies in airborne particles sampled in a control hospital room occupied by an infected subject whose viral load was also measured. Experiments were performed for two different respiratory activities – breathing and speaking.

A theoretical quantification of airborne SARS-CoV-2 RNA copy concentrations reproducing the same scenarios of the experimental analysis was also performed using a novel theoretical predictive approach which is able to predict infection risk in different indoor environments via airborne transmission (Buonanno et al., 2020a, 2020b). Finally, experimental and theoretical data were compared through a metrological compatibility analysis to provide an experimental validation of the novel predictive approach. In order to estimate the metrological compatibility, the uncertainty budget for both the experimental method and the theoretical approach was calculated.

2. Materials and methods

2.1. Experimental method to measure viral load and airborne SARS-CoV-2 concentration

To provide a direct link between the emission from an infected subject and the concentration of viable SARS-CoV-2 in air we conducted an experimental analysis measuring both (i) the viral load emission of the infected subject (i.e. the saliva viral load through an oral and nasopharyngeal swab) and (ii) the airborne SARS-CoV-2 concentration (i.e. the concentration of RNA genomic copies of SARS-CoV-2 carried by airborne respiratory particles; hereinafter referred as C_{exp}) in the infected subject's hospital room through a validated experimental method

([Robotto et al., 2021a, 2021b](#)) during two expiratory activities (breathing and speaking).

2.1.1. Measurement of the viral load

The saliva viral load of the infected subject (a 73-year-old man) was measured through an oral and nasopharyngeal swab performing a molecular test of the cycle thresholds (CT) for the two determined target genes, ORF8 and RNA-dependent RNA polymerase (RdRp). In particular, the sample is extracted with the MagMAX™ Viral/Pathogen Nucleic Acid Isolation Kit (ThermoFisher) protocol; the eluates obtained from the previous step were then analyzed in duplicate by multiplex PCR using the SARS-CoV-2 ELITe MGB Kit (ELITechGroup). Finally, the PCR analysis was performed through a QuantStudio 5 Real-Time PCR System (Applied Biosystems). The viral load, expressed as RNA concentration of the transport medium (C_{TM}, RNA copies mL^{-1}), was determined through the quantitative correlations below (Eqs. 1 and 2) between the SARS-CoV-2 reverse transcription-quantitative polymerase chain reaction (RT-qPCR) CT and the C_{TM}. The average C_{TM} for the two genes (ORF8 and RdRp) can be calculated as:

$$C_{TM-ORF8 \;\; gene} = 7 \times 10^{12} \cdot e^{-0.692 \cdot CT} \left(RNA \; copies mL^{-1} \right) \tag{1}$$

$$C_{TM-RdRp \;\; gene} = 9 \times 10^{13} \cdot e^{-0.776 \cdot CT} \left(RNA \; copies mL^{-1} \right) \tag{2}$$

The quantification curves were determined by means of a SARS-CoV-2 RNA standard (LGC Standards). The two curves (subsequently linearized to calculate the prediction intervals) were obtained with standard samples by subsequent 10-fold dilutions. The standard is LGC lot n. 70035624 and the concentration of the standard is 4.73×10^3 genome copies µL^{-1}. The pairs of values (C_{TM}-CT) adopted in the quantification curves were achieved as the average of a triplicate analysis and ranged from 26 to over 38 CT for both the target genes, then allowing a proper quantification even for low viral concentrations. A conceptual flow-chart of the methodology adopted to experimentally determine the viral load of the volunteer is reported in Fig. 2.

2.1.2. Measurement of the airborne SARS-CoV-2 concentration (C_{exp})

The experimental analysis to measure the concentration of SARS-CoV-2 RNA copies in airborne particles was conducted in a hospital room (70 m^3) at the Amedeo di Savoia Hospital (Turin, Italy) whose scheme is reported in Fig. 1. The interior door was kept open, whereas the room door and the windows were kept closed during the test. The ventilation system of the room is a simple extraction with no air recirculation: the extraction vent is placed just above the door. The air exchange rate (AER) of the room was not measured due to logistical constrains; however, Italian standards set an AER for hospital rooms in the range 2–6 h^{-1} (Repubblica, 1997; Regione Lazio, 2011): this AER
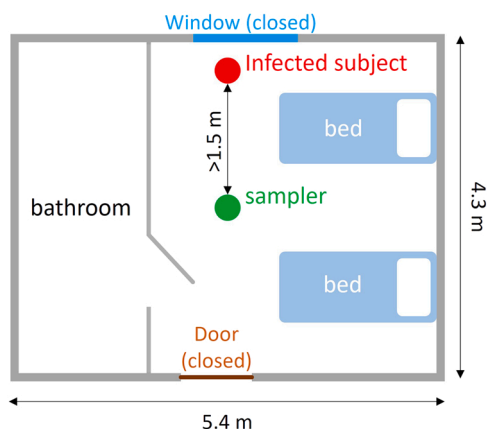

Fig. 1. Scheme of the hospital room considered for the experimental campaign; positions of the infected subject and of the sampler are also reported.

range can be considered reliable since no significant variations in design, operation, and maintenance occurred with respect to the designed value. Two emitting scenarios of the infected subject, i.e. breathing and speaking, were considered. The experiments were carried out on the basis of the following procedure: i) 20 min of background measurements (with no people in the room) followed by ii) 20 min of measurements during which the infected subject was in the room just breathing (scenario A) or speaking (scenario B).

Measurements were performed applying sampling and analytical methods considered reliable and validated according to the requirements of ISO/IEC 17025 (International Organization for Standardization, 2017). Further details of the sampling method and the experimental apparatus were reported in previous publications of the research group (Robotto et al., 2021; Robotto et al., 2021).

Airborne particles were sampled in the room air using glass-fiber filters (one for each experiment) and a high volume sampler located more than 1.5 m from the infected subject (please see Fig. 1) to avoid direct exhalations and to measure the average concentration in the room (Cortellessa et al., 2021). Amongst the different methods that can be used to sample virus-laden particles, air filtration was chosen because it is effective in both capturing submicrometric particles and collecting large air volumes at the same time. Glass-fiber filters (grade MG G, 1.5-µm pore size, 10-cm diameter, Munktell Filter AB, Falun, Sweden) were adopted rather than PTFE filters or gelatine membrane filters because their porosity allows both high flow rates and good collection efficiency. The high-volume sampler employed in the experimental analyses has a flow rate of 500 L min^{-1}, guaranteeing high analytical sensitivity. The length of the sampling (20 min) was chosen to guarantee a negligible effect of virus inactivation as reported in our previous paper (Robotto et al., 2021).

Once collected, the virus-laden particles underwent a subsequent elution step with Dulbecco's Modified Eagle's Medium (DMEM) or phosphate buffered saline (PBS) to extract the virus from the fiber solid matrix (Robotto et al., 2021). The validated operational and analytical protocol applied in the present study included the following steps:

1. air sampling for 20 min (10 m^3 of air sampled);
2. after sampling, the glass-fiber filters were immersed in 10 mL DMEM and transported to the laboratory at approximately 4 °C;
3. the glass-fiber transport medium was supplemented with a volume of fetal calf serum up to 40% of the final volume
4. samples were subjected to the combined shaking-vortexing elution protocol described by Robotto et al. (2021). Eighteen elution data sets were available with an average percentage of recovery of infectious virus, also defined as elution efficiency (ε_E), of 12.9% and a 95.4% confidence interval ranging from 2.8% to 22.9%;
5. the eluate from the glass-fiber filters was then ultracentrifuged (Optima LE-80 K, Beckman Coulter Life Science) for 1 h at 150,000 g where the viral suspension was concentrated up to 15 times. Two measurements of the recovery efficiency of ultracentrifugation, also referred to as concentration phase efficiency (ε_C), were performed and ranged from 48% to 65% (median value of 57%);
6. the supernatant was discarded and the pelleted virus was concentrated in 0.35 mL of a transport medium volume, V_{TM}, (autoclave-sterilized PBS), and the presence of SARS-CoV-2 genomic RNA was assessed and quantified by RT-qPCR.

During SARS-CoV-2 RT-qPCR, the transport medium samples were extracted with the MagMAX™ Viral/Pathogen Nucleic Acid Isolation Kit (ThermoFisher) protocol. 200 µL of each sample were resuspended in 265 µL of inactivating solution (binding solution), then magnetic beads and proteinase K were added. The extraction procedure was carried out automatically using King Fisher Flex instrumentation. At the end of the extraction process, the RNA extracted from the samples was resuspended in 50 µL of elution solution. The eluates obtained from the previous step were analyzed in triplicate by multiplex PCR using the
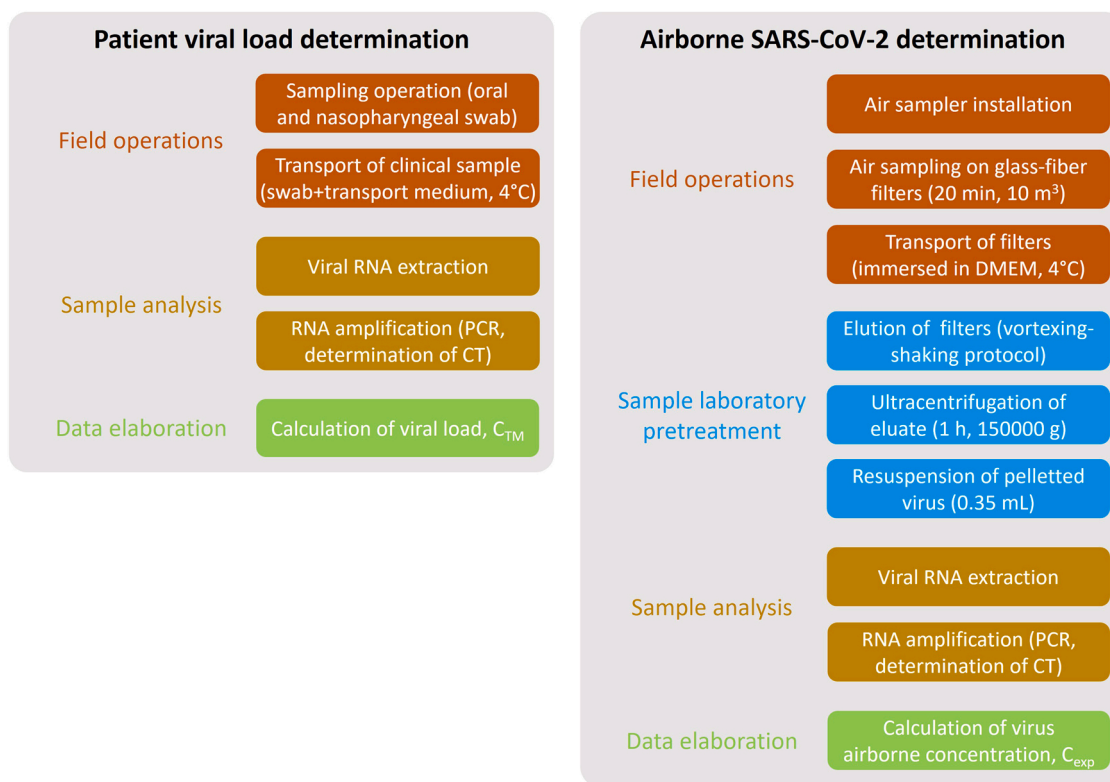
Fig. 2. Conceptual flow-charts summarizing the methodology adopted to experimentally determine the viral load of the volunteer and the airborne RNA concentration (C_{exp}) in the confined space.

SARS-CoV-2 ELITe MGB Kit (ELITechGroup). The targets were RdRp and ORF8 genes specific for SARS-CoV-2 and RNase P (RP) gene as an endogenous internal control, and the volume of sample loaded into PCR was 10 μL. The PCR analysis was performed through a QuantStudio 5 Real-Time PCR System (Applied Biosystems) and the data was processed following the instructions of the PCR kit, setting the thresholds for each individual gene and evaluating the presence of suitable PCR curves. The results were expressed with the CT values for each detected target. In cases of absence of amplification (absence of the desired target) after 40 cycles the result was reported as undetermined. We point out that environmental samples are generally characterized by very low concentration if compared to clinical samples, indeed, CT values higher than 35 are generally found by PCR. As a confirmation, Robotto et al. (2021a) reported the results of many field tests developed through a validated sampling and analytical method. They measured virus concentrations up to 50 genomic copies m^{-3} in domestic environments with poor ventilation conditions and concentrations lower than 10 genomic copies m^{-3} in hospital wards (characterized by higher air exchange rates): the corresponding CTs were in the range 35.5–39.5. Similar CT ranges were reported in other above-mentioned studies measuring similar SARS-CoV-2 airborne concentrations (Lednicky et al., 2020; Liu et al., 2020; Santarpia et al., 2020; Stern et al., 2021; Nissen et al., 2020) in hospitals. In particular, Stern et al. (2021) and Lednicky et al. (2020) reported cutoff CT values for positive air samples equal to 40.85 and 38.69, respectively. Likewise, Santarpia et al. (2020) described that the minimum environmental concentrations detected by their assay were between 39 and 44 PCR cycles; finally, Nissen et al. (2020) reported that only samples not exhibiting amplification after 45 PCR cycles were labeled as "negative". Moreover, based on our knowledge, several laboratories adopting the ELITe MGB Kit (ELITechGroup) analytical kit consider as "positive" the amplification CT up to 45.

As for the cited studies, the average RNA concentration of the transport medium (C_{TM}, copies mL^{-1}) for the ORF8 gene was calculated through the corresponding quantification curve (Eq. 1). The curve was obtained with standard samples by subsequent 10-fold dilutions; in particular, four pairs of values for both the targets were obtained (a pair of values for each dilution stage). The corresponding airborne SARS-CoV-2 concentration (C_{exp}, RNA copies m^{-3}) can be evaluated as reported in the Eq. 3; here the subscript "exp" was added to clearly indicate that this represents the average concentration resulting from the experimental analysis:

$$C_{exp} = \frac{V_{TM} \cdot 1000}{V \cdot \varepsilon_E \cdot} \varepsilon_C \cdot C_{TM} \left(\text{RNA copies m}^{-3} \right) \qquad (3)$$

where V_{TM} is the transport medium volume to be analyzed through RT-qPCR (mL), V is sampled air volume (L), ε_E is elution efficiency from the glass-fiber filters the air was filtrated through (dimensionless), and ε_C is the concentration phase efficiency by means of ultracentrifugation (dimensionless). The airborne SARS-CoV-2 concentration was evaluated considering only the ORF8 gene; thus, the $C_{TM-ORF8}$ gene quantification curve was adopted. A conceptual flow-chart of the methodology adopted to experimentally determine the airborne SARS-CoV-2 concentration is reported in Fig. 2.

2.1.3. Uncertainty budget of the experimental method

Although an estimate of the uncertainty is mandatory for accredited clinical laboratories (ISO 15189:2012 (International Organization for Standardization, 2012)), it is rarely evaluated and reported in the publication of measuring data. This could represent a critical limitation, especially in the health sector. To evaluate the uncertainty of the average RNA copy concentration, we have applied the "Guide to the expression of uncertainty in measurement" (Joint Committee for Guides in Metrology, 2008) to the relationship reported in (Eq. 3), assuming each quantity as independent. Thus, the combined standard uncertainty (u_{C-exp}) can be estimated as the square-root of the linear sum of the squared standard uncertainty components, where the *i*-th standard uncertainty component is the product of the standard uncertainty (u_i) and its associated sensitivity coefficient ($\partial C_{exp}/\partial i$). Due to the functional

relationship amongst the parameters contributing to C_{exp} (Eq. 3), the combined standard uncertainty can also be expressed as the product between the average concentration (C_{exp}) and the square-root of the linear sum of the squared standard relative uncertainty of each component (Eq. 4):

$$u_{C-exp} = \sqrt{\sum_i \left(\frac{\partial C_{exp}}{\partial i}\right)^2 \cdot (u_i)^2} = C_{exp} \sqrt{\left(\frac{u_{V_{TM}}}{V_{TM}}\right)^2 + \left(\frac{u_V}{V}\right)^2 + \left(\frac{u_{\varepsilon_E}}{\varepsilon_E}\right)^2 + \left(\frac{u_{\varepsilon_c}}{\varepsilon_C}\right)^2 + \left(\frac{u_{C_{TM}}}{C_{TM}}\right)^2} \left(\text{RNA copies} m^{-3}\right) \tag{4}$$

where $u_{V_{TM}}$, u_V, u_{ε_E}, u_{ε_c}, and $u_{C_{TM}}$ are the standard uncertainties of V_{TM}, V, ε_E, ε_C, and C_{TM}, respectively.

For elution efficiency (ε_E) and concentration phase efficiency (ε_C), the uncertainties were evaluated on the basis of the measurement results. In particular, elution efficiency data were normally distributed, whereas for the concentration phase efficiency a rectangular distribution (ranging between the two measurements) was adopted. Thus, the corresponding uncertainties were evaluated as the standard deviation of measurements divided by the square root of the number of measurements for ε_E, and as the range divided by $2\sqrt{3}$ for ε_C.

For air volume (V), a rectangular distribution was assumed within the range provided by the instrumental specifications ($\pm 5\%$), whereas for the transport medium volume (V_{TM}), a rectangular distribution was adopted on the basis of the laboratory standard and assuming a relative range of $\pm 20\%$ of the mean value.

Finally, as mentioned above, the RNA concentration of the transport medium (C_{TM}) was evaluated as a derived quantity of the CT measurements through the quantification curve for the ORF8 gene. The C_{TM} uncertainty was then evaluated as a deviation with respect to the linear regression of the CT values; in particular, $u_{C_{TM}}$ was estimated as the prediction interval (standard error of the prediction for N measures) of the linearized quantification curve, through the following equation:

$$u_{C_{TM}} = \sqrt{\left(\frac{1}{N} + \frac{1}{n}\frac{(CT - \overline{CT})^2}{S_{xx}}\right)\frac{SS_R}{n-2}} \left(\text{RNA copies} m^{-1}\right) \tag{5}$$

where:

- CT is the current CT value, obtained by means of RT-qPCR, determined as the average value of N readings (with N ranging from 1 to 3 in the present analysis as a function of the concentration, and considering that low concentrations did not allow adopting higher N);
- $\overline{CT}$ is the mean value of the CTs obtained by subsequent 10-fold dilution of the SARS-CoV-2 RNA standard;
- n is the number of measures (pairs) performed to obtain the quantification curve (four couples of measurements were performed in the present study due to the low concentration under investigation);
- SS_R is the sum of squares of residuals;
- $S_{xx} = \sum_{i=1}^n (CT_i - \overline{CT})^2$, where CT_i is the CT corresponding to each RNA standard dilution for which the quantification curve is obtained.

The sensitivity coefficients of each input parameter ($\partial C_{exp}/\partial i$) were numerically evaluated, as stated in Annex B of the "Guide to the expression of uncertainty in measurement" (Joint Committee for Guides in Metrology, 2008), by holding all input quantities but one (the i-th) fixed at their best estimates. Once the standard uncertainty u_{C-exp} was estimated, the expanded uncertainty, with a 95.4% confidence interval (coverage factor of 2), was calculated as:

$$U_{C-exp} = 2 \cdot u_{C-exp} \left(\text{RNA copies} m^{-3}\right) \tag{6}$$

2.2. Theoretical approach to estimate the airborne SARS-CoV-2 concentration (C_{theor})

The theoretical approach is based on a emission-to-risk approach recently developed by the authors (Buonanno et al., 2020a; Buonanno et al., 2020b; Mikszewski et al., 2021). The novel aspect of the approach lies in a predictive emission approach to estimate the viral load emission rate (E_{vl}) of an infected subject on the basis of the viral load (C_{TM}, RNA copies mL^{-1}), the airborne particle volume concentration expelled by the infectious person during different activities (i.e. breathing, speaking, singing, etc.) (V_d, mL m^{-3}), and the flow rate expired as a function of the activity level (inhalation rate, IR, m^3 h^{-1}).

$$E_{vl} = C_{TM} \cdot IR \cdot V_d \left(\text{RNA copies} h^{-1}\right) \tag{7}$$

The authors point out that the predictive emission approach is a key aspect since the issue of the viral load emitted was difficult to solve and, in the past, backward calculation was used to estimate the emission of an infected subject based on retrospective assessments of infectious outbreaks only at the end of an epidemic (Sze and Chao, 2010; Wagner et al., 2009; Rudnick and Milton, 2003). The forward emission approach allowed for the first time the accurate simulation and prediction of infection risk in different indoor environments via airborne transmission both in close proximity situations (e.g. through complex computational fluid dynamics analyses (Cortellessa et al., 2021; Dbouk and Drikakis, 2020; Dbouk and Drikakis, 2020; Dbouk and Drikakis, 1994)) and in indoor environments (e.g. adopting simplified zero-dimensional models (Buonanno et al., 2020; Mikszewski et al., 2021; Stabile et al., 2021)). Indeed, applying a mass balance approach (i.e. a zero-dimensional model which considers fully mixing conditions), the indoor SARS-CoV-2 concentration over time (hereinafter referred as $C_{theor}(t)$, RNA copies m^{-3}) can be estimated through the theoretical approach as reported in the Eq. (8). Here the subscript "theor" was adopted to clearly indicate that this represents the concentration resulting from the theoretical approach and to differentiate it from experimentally measured concentrations:

$$\frac{dC_{theor}(t)}{dt} = \frac{E_{vl}}{V_{room}} - IVRR \cdot C_{theor}(t) \left(\text{RNA copies} m^{-3}\right) \tag{8}$$

We point out that the fully mixing condition cannot be experimentally checked for practical and metrological reasons (e.g. we should have adopted several sampling points in a hospital ward in the presence of an infected person). Nonetheless, several theoretical and numerical studies have demonstrated that the droplet and pollutant concentrations as well as the risk of infection are affected by the distance from the source only in the close proximity of the source, which was evaluated roughly equal to 1.5 m (Cortellessa et al., 2021; Chen et al., 2020; Li, 2021). Beyond that distance the concentration/risk can be considered homogeneously distributed at least for distances higher than those characteristics of the investigated ward (Lakey et al., 2021). In the case of initial concentration equal to 0, the indoor SARS-CoV-2 concentration can be estimated as:

$$C_{theor}(t) = \frac{E_{vl}}{V_{room} \cdot IVRR} \left(1 - e^{-IVRR \cdot t}\right) \left(\text{RNA copies} m^{-3}\right) \tag{9}$$

where *IVRR* (h^{-1}) represents the infectious virus removal rate in the space investigated and V$_{room}$ (m^3) is the volume of the indoor environment considered. The infectious virus removal rate is the sum of three contributions (Yang and Marr, 2011): the AER (h^{-1}) via ventilation, the particle deposition on surfaces (k, h^{-1}) and the viral inactivation (λ, h^{-1}).

Thus, the 20-min average RNA concentration (C$_{theor}$) to be compared with the measured concentrations in the two abovementioned scenarios is determined as:

$$C_{theor} = \int_{T} C_{theor}(t)dt$$

$$= \frac{E_{vl}}{V_{room} \cdot IVRR} \left[1 - \frac{1}{IVRR \cdot T} \cdot \left(1 - e^{-IVRR \cdot T}\right) \right] \left(RNA\ copies\,m^{-3} \right)$$

(10)

with T total duration of the event (20 min). A conceptual flow-chart summarizing the methodology adopted to calculate the average RNA concentration (C$_{theor}$) is shown in Fig. 3, here parameters and models in the calculation are reported.

A Monte Carlo simulation (Hammersley and Handscomb, 1964) was run to estimate the RNA copy concentration in both the scenarios given a range of input values through the predictive estimation approach (Buonanno et al., 2020a). To this end, probability distribution functions and related values of the different parameters were adopted based on the measurements carried out in the present study or obtained from the scientific literature as summarized in Table 1. All the parameters were assumed to be uncorrelated and Monte Carlo simulations were run performing 1×10^6 trials to estimate the average RNA copy concentration (C$_{theor}$).

For the viral load (C$_{TM}$), a rectangular (i.e. uniform) distribution of the data, ranging from 2.4×10^6 to 5.5×10^6 RNA copies mL^{-1} was considered on the basis of the values obtained from the SARS-CoV-2 molecular test of the subject (reported in Section 3.1). For the inhalation rate, the data reported in the scientific literature (Adams, 1993; International Commission on Radiological Protection, 1994) for sitting

Table 1

Probability distribution of the parameters used to calculate average viral indoor concentration: normal distributions were reported as average values ± standard deviation, whereas rectangular distributions were reported as median value and minimum-maximum range.

Parameter	Distribution	Distribution parameters	references
Viral load, C$_{TM}$ (RNA copies mL^{-1})	Rectangular	4.0×10^6 ($2.4 \times 10^6 - 5.5 \times 10^6$)	Measured, this study (see Section 3.1)
Inhalation rate while standing, IR (m^3 h^{-1})	Rectangular	0.52(0.47 – 0.57)	(Adams, 1993; International Commission on Radiological Protection, 1994)
Particle volume while speaking, V$_{D-speaking}$ (mL m^{-3})	Rectangular	6.6×10^{-3}($1.2 \times 10^{-3} - 1.2 \times 10^{-2}$)	Duguid (1945); Evans (2020); Johnson et al. (2011)
Particle volume while breathing, V$_{D-breathing}$ (mL m^{-3})	Rectangular	1.0×10^{-3}($1.0 \times 10^{-6} - 2.0 \times 10^{-3}$)	(Buonanno et al. (2020); Morawska et al. (2009)
Room volume, V$_{room}$ (m^3)	Normal	70.0 ± 0.7	Measured, this study (adopting an uncertainty of 2% according to Ambrosio Alfano et al., 2012)
Air exchange rate, AER (h^{-1})	Rectangular	4.0(2.0 – 6.0)	Italian standard (Repubblica, 1997; Regione Lazio, 2011)
Particle deposition rate, k (h^{-1})	Log-normal	$\log_{10}(-0.62) \pm \log_{10}(0.30)$	Chatoutsidou and Lazaridis (2019)
Inactivation rate, λ (h^{-1})	Rectangular	0.32(0 – 0.63)	Fears et al. (2020); van Doremalen et al. (2020)
Time fraction of speaking, TF$_{speaking}$ (-)	Rectangular	0.8(0.6–1.0)	Estimated, this study
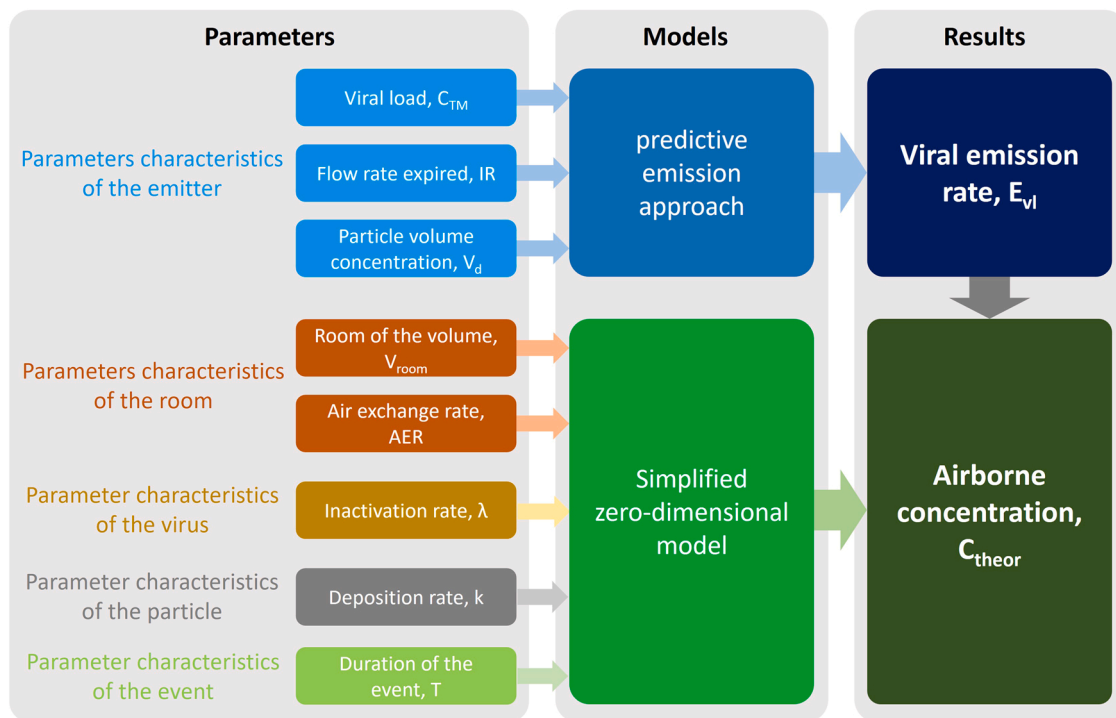
Fig. 3. Conceptual flow-chart summarizing the methodology adopted to calculate the average RNA concentration (C$_{theor}$) in the confined space: parameters and models adopted in the calculation are reported.

activity levels were collected: the values ranged between 0.47 and 0.57 $m^3 h^{-1}$ and a rectangular probability distribution was considered.

Experimental data from the scientific literature are not definitive for the particle volume emitted (V_d), because the sampling method itself can affect the results due to the rapid dehydration of the large particles emitted (Yang and Marr, 2011; Abbas and Pittet, 2020; Morawska and Buonanno, 2021; Stadnytskyi et al., 2020). Still today the understanding of the initial instant of respiratory particle emission is not definitive and does not lead to conclusive answers, mainly due to the complexity of physical processes such as evaporation and the difficulty of measuring particle emissions in situ (Bake et al., 2019, 2017). As a consequence, V_d was found to range from roughly 1.2×10^{-3} to 1.2×10^{-2} mL m^{-3} for speaking ($V_{D\text{-speaking}}$, (Duguid, 1945; Evans, 2020; Johnson et al., 2011)) and from 1.0×10^{-6} to 2×10^{-3} for breathing ($V_{D\text{-breathing}}$, (Buonanno et al., 2020; Morawska et al., 2009)). Rectangular probability distributions were applied to those data in the Monte Carlo simulations. The room volume (V) was measured as 70 m^3: volume values with a normal probability distribution were generated in the Monte Carlo simulations adopting an expanded uncertainty of 2% as estimated by d'Ambrosio Alfano et al. (2012).

AER data were generated adopting a rectangular probability distribution function with values ranging from 2.0 to 6.0 h^{-1} as mentioned above. Similarly, the inactivation rate (λ) was considered equiprobable and ranging from 0 h^{-1} (Fears et al., 2020) to 0.63 h^{-1} (van Doremalen et al., 2020). In contrast, the deposition rate (k) is a function of the particle size; thus, on the basis of the settling velocity provided in Chatoutsidou and Lazaridis (2019) for particles < 10 μm, a log-normal distribution function with an average value of $\log_{10}(-0.62)$ (i.e. 0.24 h^{-1}) was considered.

Finally, for the scenario with the subject speaking for 20 min (scenario B), an actual time fraction of speaking (TF$_{speaking}$) was estimated and adopted to take into account the subject's involuntary pauses during speaking. In other words, the total length (20 min) was multiplied by a TF$_{speaking}$ ranging from 0.6 to 1.0 (rectangular distribution function). During the corresponding remaining fraction of the time (0.4–0, respectively) the patient was considered to be just breathing and the corresponding particle volume ($V_{D\text{-breathing}}$, particle volume emitted while breathing) was applied.

2.2.1. Uncertainty budget of the theoretical approach

The Monte Carlo simulations and the corresponding uncertainty budgets were carried out adopting Supplement 1 to the "Guide to the expression of uncertainty in measurement" (Joint Committee for Guides in Metrology, 2008). In particular, the expanded uncertainty range was expressed as 95.4% confidence interval (coverage factor of 2) of the simulation results obtained from the 10^6 trials.

The contribution of each input parameter to the overall RNA concentration uncertainty was also evaluated by adopting a Monte Carlo simulation (instead of an analytical approach), as suggested in Annex B of Supplement 1 to the "Guide to the expression of uncertainty in measurement" (Joint Committee for Guides in Metrology, 2008). Indeed, we have evaluated the percent contribution of each i-th component as:

$$\left(\frac{\partial C_{theor}}{\partial i}\right)^2 \bullet (u_i)^2 \Bigg/ \left[\sum_i \left(\frac{\partial C_{theor}}{\partial i}\right)^2 \bullet (u_i)^2\right] \left(-\right) \tag{11}$$

where ($\partial C_{theor}/\partial i$) and u_i represent the sensitivity coefficient and the standard uncertainty of the i-th component, respectively. The sensitivity coefficients were numerically evaluated by holding all input quantities but one (the i-th) fixed at their best estimates, whereas the uncertainty of the i-th component was evaluated with a 68.3% confidence interval (i.e. adopting the standard deviation in cases of normal distributions and the range divided by $2\sqrt{3}$ in cases of rectangular distributions).

2.3. Metrological compatibility

The in-depth metrological analysis of the experimental method (Section 2.1.3) and the numerical evaluation of the theoretical approach (Section 2.2.1) in estimating the uncertainty of the airborne SARS-CoV-2 concentration were aimed at evaluating the metrological compatibility between experimental and theoretical data (Joint Committee for Guides in Metrology, 2008).

The authors point out that metrological compatibility allows a conformity assessment to be made; that is, deciding if an item of interest conforms to a specified requirement. Indeed, two measurements of the same magnitude can be different, but metrologically compatible (i.e. not statistically different), if their difference falls within the experimental error considering the corresponding uncertainties or if there is a value that falls within both measurement ranges. In this paper, we apply the principles of the conformity assessment to the RNA copy concentration obtained through the experimental methodology and the predictive approach as reported in the ISO/IEC 17043 standard (International Organization for Standardization, 2010). The compatibility is assured if the absolute value of the difference of any pair of measured quantity values (mean values) from two different measurement results is smaller than the expanded measurement uncertainty of that difference. In other words, the metrological compatibility of measurement results replaces the traditional concept of 'staying within the error', as it represents the criterion to decide whether two measurement results refer to the same measurand or not (International Organization for Standardization, 2010). Metrological compatibility is determined in terms of normalized error E_n (to be less than 1), defined on the basis of the above-reported uncertainties (Joint Committee for Guides in Metrology, 2008) as:

$$E_n = \frac{|C_{exp} - C_{theor}|}{\sqrt{U_{C-exp}^2 + U_{C-theor}^2}} < 1 \left(-\right) \tag{12}$$

where C and U_C are the mean values and the expanded uncertainties referred to in the data obtained through the experimental method ($U_{C\text{-exp}}$) or the theoretical approach ($U_{C\text{-theor}}$). While the uncertainty range of the experimental data is symmetric with respect to average value, as reported in the results, the uncertainty range resulting from the theoretical approach is asymmetric with respect to the median value (see Section 3.2). In view of a conservative approach, the normalized error was calculated considering the smallest value amongst (i) the difference between the highest value of the confidence interval and the median value and (ii) the difference between the lowest value of the confidence interval and the median value.

3. Results and discussions

3.1. Results of the experimental analysis and uncertainty budget

The molecular test performed through the oral and nasopharyngeal swab samples of the infected subject resulted in CT values for the two target genes, ORF8 and RdRp, of 21.51 and 21.41, respectively; thus, the corresponding RNA concentration of the transport medium (C_{TM}), evaluated through the quantification curves (Eqs. 1–2), ranged between 2.4×10^6 and 5.5×10^6 RNA copies mL^{-1} (median value of 4.0×10^6 RNA copies mL^{-1}).

The concentrations of airborne SARS-CoV-2 for scenarios A and B are reported in Table 2 and Fig. 4. A very low or undetectable concentration of airborne RNA copies was measured during scenario A, suggesting that the ventilation supplied in hospital rooms was effective in limiting the airborne transmission of SARS-CoV-2 when the infected person was just breathing due to the lower emissions typical of such expiratory activity. Such an undetectable concentration was somehow expected because the minimum detection threshold of the experimental device is around 2 RNA copies m^{-3} and because during breathing, an infected subject emits

Table 2

Average airborne SARS-CoV-2 concentrations (C_{exp}) and expanded uncertainty (U_{C-exp}) resulting from the experimental analysis for both the scenarios considered. Cycle threshold (CT) and C_{TM} values for the endogenous gene RP (adopted for internal control) and for the gene ORF8 (adopted to calculate the concentration through the quantification curve) are also reported.

Experiment/ scenario	Respiratory activity	CT for endogenous gene target (RP)	CT for virus gene target (ORF8)	C_{TM} (RNA copies mL^{-1})	C_{exp} (RNA copies m^{-3})	U_{C-exp} (RNA copies m^{-3})
A	Breathing	38.42	Undetermined	Undetermined	Undetermined	Undetermined
B	Speaking	38.59	37.16	34.06	16.1	32.8
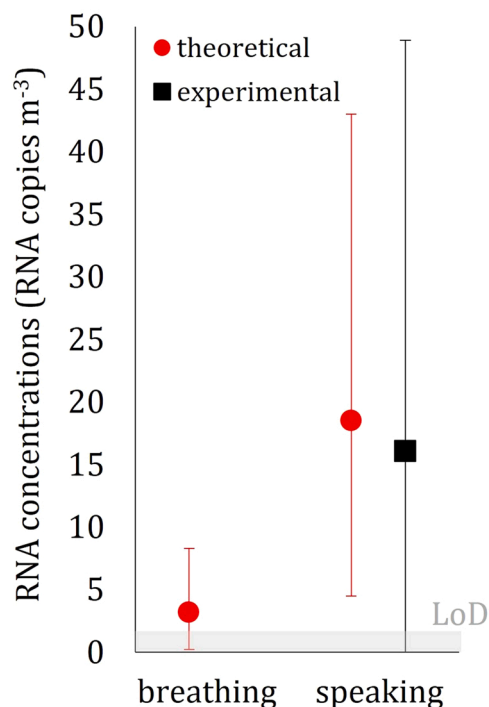
Fig. 4. Average airborne RNA concentration measured through the experimental analysis and estimated through the theoretical approach for both breathing and speaking scenarios; expanded uncertainty bars and limit of detection of the experimental apparatus (LoD) are also reported.

about 10 times less than during speaking (Morawska et al., 2009). In contrast, the concentration measured during scenario B was much higher; in this case, with a speaking subject, a value of 16.1 RNA copies m^{-3} was measured. We point out that the reliability of the RNA concentration for such high CT values is confirmed by our previous papers where a high number of experimental data were provided (Robotto et al., 2021a, 2022, 2021b,). This value is within the range of values (1–100 RNA copies m^{-3}) measured in hospital wards in previous researches (Lednicky et al., 2020; Liu et al., 2020; Santarpia et al., 2020; Stern et al., 2021), confirming the presence of virus-laden particles in this type of microenvironments even beyond close proximity to an infected subject. These data highlight the relevance of vocalization in

terms of viral load emission and, consequently, of RNA copy concentration in the environment. In fact, the virus-laden particles emitted from the human respiratory tract are generated by aerosolization (i.e. by turbulent flows stripping particles from a fluid film) and by a fluid film or bubble burst process while vocal cords adduct and vibrate during speaking (Johnson et al., 2011). In particular, speaking activity was proven to emit additional particles in respect to breathing in modes near 3.5 and 5 μm, suggesting that the aerosolization of secretions lubricating the vocal chords is a major source of particles in terms of number (Morawska et al., 2009).

The expanded uncertainty (U_{C-exp}, coverage factor of 2) for scenario B, resulting from the evaluation described in Section 2.1.3, was equal to 32.8 RNA copies m^{-3} (i.e. a relative expanded uncertainty of 204%). Such a huge uncertainty highlights the complexity of the RNA copy concentration measurement and underlines the importance of estimating the uncertainty value for this type of measurement: indeed, like most of the measurements in the medical field, the uncertainty of the RNA copy concentration measurement is typically not provided. The reason for the high uncertainty is expressed by the relative contributions (uncertainty weights) of the parameters contributing to the uncertainty U_{C-exp}. These contributions, along with sensitivity coefficients and standard uncertainties of each parameter, are summarized in Table 3. In particular, the main contributions to overall uncertainty (scenario B) are due to two parameters: C_{TM}, with a relative contribution of 84.9%, and ε_C, with a relative contribution of 13.7%. The C_{TM} uncertainty is calculated by means of well-known models valid for the standard error of the prediction reported in (Eq. 5); in particular, the quantification curve is based on four pairs of measures (expressed as *n* in (Eq. 5)) each of which is performed with 1–3 readings (expressed as *N* in (Eq. 5)). Thus, the uncertainty could be hypothetically reduced only by increasing the number of standard dilutions and readings. Nonetheless this is not practically suitable when low concentrations are measured, in which case neither further 10-fold dilutions nor further readings at each dilution stage can be applied. Similarly, the mean value of the concentration efficiency ε_C was obtained from just two measurements, so its uncertainty could be reduced by increasing the number of ultracentrifugation assays.

The authors point out that for the typical concentration values occurring in real life environments (i.e. < 100 RNA copies m^{-3}), a very large uncertainty is expected. Indeed, in that concentration range, the effect of the actual concentration on the uncertainty is negligible. This is clearly shown in Fig. 5a where the relative uncertainty as a function of the concentrations was calculated and reported: the uncertainty is
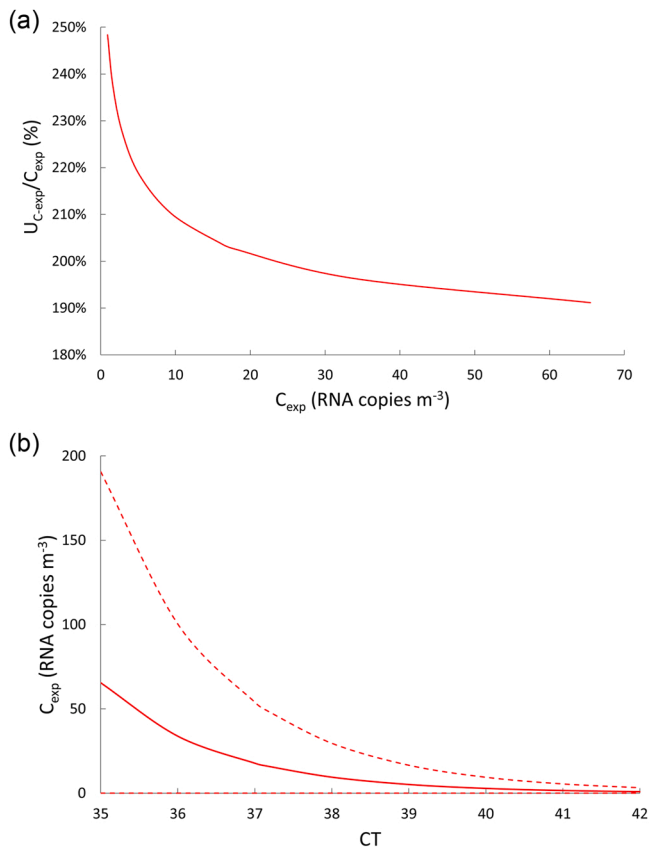
Table 3

Distribution of the parameters measured to calculate C_{exp} and their sensitivity coefficients, standard uncertainties and contributions (weights) to the overall uncertainty (U_{C-exp}). Normal distributions were reported as average values ± standard deviation, whereas rectangular distributions were reported as median value and minimum-maximum range.

Parameter	Distribution parameters	Probability distribution	Sensitivity coefficient ($\partial C_{exp}/\partial i$)	Standard uncertainty (u_i)	Uncertainty weight (%)
ε_E	12.9% ± 5.0%	Normal	-28.22 RNA copies m^{-3}/(-)	0.0118 (-)	< 0.1%
ε_C	57% (48–65%)	Rectangular	-123.75 RNA copies m^{-3}/(-)	0.049 (-)	13.7%
V	10 m^3 (9.5–10.5 m^3)	Rectangular	-0.0016 RNA copies m^{-3}/(L)	288.68 L	0.1%
V_{TM}	0.35 (0.28–0.42) mL	Rectangular	45.96 RNA copies m^{-3}/(mL)	0.04 mL	1.3%
C_{TM}	34.06 (17.57–66.04) RNA copies mL^{-1}	Not available	0.472 RNA copies m^{-3}/(RNA copies mL^{-1})	31.98 RNA copies mL^{-1}	84.9%

Fig. 5. Trends of: (a) estimated relative expanded uncertainty ($U_{C\text{-exp}}/C_{exp}$) as a function of the RNA copy concentrations, and (b) RNA copy concentrations (C_{exp}) as a function of the cycle threshold (CT) values (solid line represents the average values, whereas dashed lines represent 95.4% confidence interval values).

extremely high (> 190%) over the entire concentration range analyzed. Analogously, in Fig. 5b the RNA copy concentrations (and the corresponding uncertainty ranges) as a function of the CT values are also reported. The trend shows that, as previously reported, the measured CT value of 37.16 corresponds to a C_{exp} of 16.1 RNA copies m^{-3} with a 95.4% confidence range of 0–48.9 RNA copies m^{-3} (i.e. $U_{C\text{-exp}} = 32.8$ RNA copies m^{-3}) and how for lower CT values (i.e. for higher airborne concentrations) the relative confidence interval remains roughly constant.

3.2. Results of the theoretical approach and uncertainty budget

In Table 4, the average RNA concentrations (C_{theor}) estimated through the Monte Carlo simulations for scenarios A and B (infected subject breathing and speaking) are reported along with the expanded uncertainty range (95.4% confidence interval, coverage factor of 2) and the sensitivity coefficients. The median values were equal to 3.2 RNA copies m^{-3} (with 95.4% confidence interval equal to 0.2–8.3 RNA copies m^{-3}) and 18.5 RNA copies m^{-3} (with 95.4% confidence interval equal to 4.5–43.0 RNA copies m^{-3}) for breathing and speaking scenarios, respectively. The contributions of each input parameter to the overall RNA concentration uncertainty, evaluated adopting the Monte Carlo simulation as suggested by the Guide to the expression of uncertainty in measurement (Joint Committee for Guides in Metrology, 2008) and described in Section 2.2.1, are also reported. Such an uncertainty budget provides key information as it clearly highlights which parameter most affects the uncertainty of the RNA concentration.

The main contributions of the speaking scenario (scenario B) were the particle volume emission while speaking (75.4%) and the viral load

Table 4
Results of indoor RNA concentrations obtained through Monte Carlo simulations for breathing (scenario A) and speaking (scenario B). Data are expressed as median values and range of the corresponding expanded uncertainties (95.4% confidence interval). The sensitivity coefficients, the standard uncertainties (u_i) and the contributions of the i-th parameter to the overall RNA concentration uncertainties are also reported.

C_{theor} (RNA copies m^{-3})			Scenario A (breathing)	Scenario B (speaking)
			3.2 (0.2–8.3)	18.5 (4.5–43.0)
Parameter	**Sensitivity coefficients** ($\partial C_{theor}/\partial i$)	**Standard uncertainty** (u_i)	**Uncertainty weight (%)**	
C_{TM}	Scenario A: 5.0×10^{-6} RNA copies m^{-3}/(RNA copies mL^{-1}) Scenario B: 8.6×10^{-7} RNA copies m^{-3}/(RNA copies mL^{-1})	9.0×10^5 RNA copies mL^{-1}	13.0%	19.0%
IR	Scenario A: 0.06 RNA copies m^{-3}/(m^3 h^{-1}) Scenario B: 36.67 RNA copies m^{-3}/(m^3 h^{-1})	0.03 m^3 h^{-1}	< 0.1%	1.0%
$V_{D\text{-speaking}}$	Scenario A: - Scenario B: 2888.1 RNA copies m^{-3}/(mL m^{-3})	0.0031 mL m^{-3}	–	75.4%
$V_{D\text{-breathing}}$	Scenario A: 3373.6 RNA copies m^{-3}/(mL m^{-3}) Scenario B: 904.5 RNA copies m^{-3}/(mL m^{-3})	0.0006 mL m^{-3}	84.5%	0.3%
V_{room}	Scenario A: − 0.048 RNA copies m^{-3}/(m^3) Scenario B: − 0.286 RNA copies m^{-3}/(m^3)	0.70 m^3	< 0.1%	< 0.1%
AER	Scenario A: − 0.271 RNA copies m^{-3}/(h^{-1}) Scenario B: − 1.235 RNA copies m^{-3}/(h^{-1})	1.15 h^{-1}	2.2%	1.9%
$\log_{10}k$	Scenario A: − 0.305 RNA copies m^{-3}/(h^{-1}) Scenario B: − 1.455 RNA copies m^{-3}/(h^{-1})	0.30 h^{-1}	0.2%	0.2%
λ	Scenario A: − 0.305 RNA copies m^{-3}/(h^{-1}) Scenario B: − 1.454 RNA copies m^{-3}/(h^{-1})	0.18 h^{-1}	0.1%	0.1%
$TF_{speaking}$	Scenario A: - Scenario B: 13.146 RNA copies m^{-3}/(-)	0.12 (-)	–	2.1%

(19.0%), analogously, for the breathing scenario (scenario A), the main contributions were the particle volume while breathing (84.5%) and the viral load (13.0%); for both the scenarios the other contributions were much lower or even negligible. As an example, the uncertainty weight of the AER is just about 2% even if a quite large range (2–6 h^{-1}) was

adopted in the calculations. Indeed, for such short experiments (20-min) the effect of the AER on the RNA concentration is well within the uncertainty related to the other parameters. This is clearly confirmed by the sensitivity coefficients reported in Table 4: for speaking activity the AER sensitivity coefficient is -1.235 RNA copies m^{-3}/h^{-1}, thus, for ± 2 h^{-1} with respect to the adopted average value (4 h^{-1}), the RNA concentration would be just ± 2.470 RNA copies m^{-3}. Therefore, even if the AER of the room was not measured due to logistical constrains (as mentioned above), the quite large AER range suggested by the Italian standards does not significantly influence the experimental results and the findings of the paper.

The authors point out that when the viral load is not measured (unlike the present study), its contribution to the RNA concentration uncertainty would become even larger as the C_{TM} of the infected person can potentially range over several orders of magnitude (Pan et al., 2020) and, consequently, the standard uncertainty will also greatly increase.

3.3. Metrological compatibility

On the basis of the average airborne SARS-CoV-2 concentrations measured through the experimental analysis (C_{exp}) and estimated through the theoretical approach (C_{theor}), as well as of the corresponding uncertainties (U_{C-exp} and $U_{C-theor}$, respectively), the normalized error E_n (Eq. 12) was evaluated to assess the metrological compatibility amongst the experimental and theoretical results. In scenario B (infected subject speaking), E_n was much lower than 1 (0.06), thus revealing excellent metrological compatibility.

The authors point out that metrological compatibility can be obtained (and, indeed, it was expected) when such large uncertainty ranges are estimated (both experimentally and theoretically); thus, just reporting the E_n value to claim metrological compatibility could downplay the actual findings of the paper. Indeed, it should be highlighted that for scenario B (where both experimental and theoretical data are available) the difference amongst the average concentrations, i. e. the numerator of E_n, ($C_{exp} = 16.1$ RNA copies m^{-3}, $C_{theor} = 18.5$ RNA copies m^{-3}) is extremely low and it would guarantee a metrological compatibility ($E_n < 1$) even for very low, and technically unfeasible, uncertainties of $\pm 10\%$. Thus, having pointed this out, the present paper does represent an experimental validation of the predictive estimation approach for the RNA copy emission rate previously developed by the authors. Such validation is extremely important because the viral emission approach represents a major step towards predicting infection risk in different indoor environments via airborne transmission. Indeed, previous studies were performed adopting emission rates obtained from rough estimates based on retrospective assessments of infectious outbreaks only at the end of an epidemic (Rudnick and Milton, 2003; Wagner et al., 2009). In fact, such an emission approach, adopted in retrospective assessments, was able to reproduce the attack rate of a documented outbreak due to airborne transmission (Buonanno et al., 2020; Miller et al., 2020). Nonetheless, a proper validation of the approach has not yet been performed.

For scenario A (infected subject breathing), it was not possible to estimate the normalized error E_n because the experimental concentrations were lower than the instrumental limit of detection. Thus, as mentioned above, we can infer that the experimental concentration was < 2 RNA copies m^{-3}; therefore, we can just report that it is within the confidence interval estimated through the theoretical approach (0.2–8.3 RNA copies m^{-3}). Longer emission periods or lower ventilation rates would have likely allowed higher, and then detectable, indoor airborne concentrations and would have allowed a proper validation of the theoretical approach also for low emitting expiratory activities.

The metrological compatibility assessment also highlighted the importance of estimating the uncertainty value for this type of measurement and the need to reduce it; indeed, even if a large uncertainty can be expected and accepted for simplified theoretical approaches, it cannot be tolerated for experimental measurement in the medical field.

Therefore, this first-time estimation of the uncertainty (and the relative contributions) of this experimental analysis represents a key step in the process of improving the measurement method for the airborne concentration of respiratory viruses.

3.4. Limitations and research opportunities

The findings of the paper here shown represent a key step forward for a proper acknowledgement of the airborne transmission of respiratory viruses as it is the very first experimental proof of this mode of transmission. The complexity of the experimental analysis here presented clearly testifies some weaknesses that represent simultaneously limitations and research opportunities for future studies. The main criticality is the limited number of tests performed: two single tests (one for each expiratory activity) can be considered enough for this first study, where a direct emission-to-concentration link was performed for the very first time, but future studies should rely upon different tests allowing reducing the measurement uncertainty. Moreover, in the case of low emitting activities, such as breathing, particular attention should be paid when designing the experiments. Indeed, duration of the event, room volume and air exchange rate should be properly chosen in order to obtain "measurable" concentrations. Finally, in order to validate the theoretical approach also for other expiratory activities, experiments considering activities claimed to be extremely high emitting, e.g. loudly speaking, sneezing, coughing, should be performed.

4. Conclusions

Although the detection of SARS-CoV-2 RNA copies in airborne particles has been previously reported, including in hospital wards, no studies in the scientific literature have provided a direct link between the emission of RNA copies from an infected subject and the concentration of viable SARS-CoV-2 in the air. To fill this gap, an experimental analysis was conducted under controlled conditions in a hospital room to measure both the viral load of an infected subject (through an oral and nasopharyngeal swab) and the SARS-CoV-2 RNA copies in airborne particles while the subject was breathing and speaking. Additionally, a novel predictive theoretical approach recently developed by the authors was also applied to the same scenarios to validate it through a metrological compatibility analysis against the experimental results. To assess the metrological compatibility for both the experimental method and the theoretical approach, an uncertainty budget was developed.

The key findings can be summarized as follows:

1. For a measured viral load of the infected subject in the range of 2.4×10^6 to 5.5×10^6 RNA copies mL^{-1}, the corresponding average airborne SARS-CoV-2 concentration while the subject was speaking was equal to 16.1 RNA copies m^{-3}, whereas for breathing, the concentration was lower than the detection limit of the instrumental apparatus (i.e. < 2 RNA copies m^{-3}).
2. The airborne SARS-CoV-2 concentrations estimated by the novel predictive estimation approach were 18.5 and 3.2 RNA copies m^{-3} for speaking and breathing, respectively. Thus, the concentration estimated for speaking scenario was in excellent agreement with the measured value as verified by the metrological compatibility analysis.

Consequently, the following conclusions can be drawn from the experimental and theoretical results:

1. *A direct link between emission and airborne concentration was demonstrated when the subject was speaking.* The study established that the virus is airborne with consequent risk of contagion when a susceptible subject inhales infectious quanta of the virus contained in particles from respiratory activities.

2. *Inability to detect the presence of the virus in the air (in terms of RNA copies) when the subject was breathing does not mean that there is no infection risk when people are not vocalizing.* The concentration of the virus below the method detection limit does not exclude the possibility of inhalation of infectious quanta during longer exposures in poorly ventilated environments.

3. *The link between emissions and airborne concentrations can be quantified by means of a recently developed theoretical approach.* The study validated the theoretical approach through a metrological compatibility analysis, suggesting that it can support public health authorities in deciding on control measures to lower the infection risk. For example, simulation of exposure scenarios (both in close proximity and indoor environments) enables the maximum occupancy of indoor environments under consideration (e.g., classrooms, transport microenvironments) and the maximum duration of the occupancy (events) to be determined.

4. *The complex nature of the experimental method required to measure the airborne SARS-CoV-2 concentration is unavoidably associated with high uncertainties.* The uncertainty evaluation of the experimental method conducted in this study is of great significance because, for the first time, it was possible to identify which parameters are key contributors to the uncertainty.

5. *The uncertainty budget of the theoretical approach identified the volume particle emission (if the viral load is measured) as the main contributor to the uncertainty.* This means that improving the accuracy of the measurement of the respiratory particles emitted during different activities, which represents a key challenge for the scientific community involved in this type of research, could reduce the overall uncertainty of the predictive approach.

CRediT authorship contribution statement

G. Buonanno: Conceptualization, Writing – review & editing, Project administration. **A. Robotto:** Conceptualization, Writing – review & editing. **E. Brizio:** Writing – original draft, Investigation, Methodology. **L. Morawska:** Writing – review & editing, Supervision. **A. Civra:** Data curation, Methodology. **F. Corino:** Writing – original draft, Investigation. **D. Lembo:** Investigation, Validation, Methodology. **G. Ficco:** Data curation, Validation. **L. Stabile:** Writing – original draft, Investigation, Formal analysis.

Declaration of Competing Interest

The authors declare that they have no known competing financial interests or personal relationships that could have appeared to influence the work reported in this paper.

References

Abbas, M., Pittet, D., 2020. Surfing the COVID-19 scientific wave. Lancet Infect. Dis. S1473–3099 (20), 30558–30562. https://doi.org/10.1016/S1473-3099(20)30558-2.

Adams, W.C., Measurement of Breathing Rate and Volume in Routinely Performed Daily Activities. Final Report. Human Performance Laboratory, Physical Education Department, University of California, Davis., Human Performance Laboratory, Physical Education Department, University of California, Davis. Prepared for the California Air Resources Board, Contract No. A033–205, April 1993., 1993.

Bake, B., Ljungström, E., Claesson, A., Krage, C., Holm, M., Olin, A.C., 2017. Exhaled particles after a standardized breathing maneuver. J. Aerosol Med. Pulm. Drug Deliv. 30, 267–273.

Bake, B., Larsson, P., Ljungkvist, G., Ljungström, E., Olin, A.-C., 2019. Exhaled particles and small airways. Respir. Res. 20, 8. https://doi.org/10.1186/s12931-019-0970-9.

Buonanno, G., Stabile, L., Morawska, L., 2020. Estimation of airborne viral emission: quanta emission rate of SARS-CoV-2 for infection risk assessment. Environ. Int. 141, 105794 https://doi.org/10.1016/j.envint.2020.105794.

Buonanno, G., Morawska, L., Stabile, L., 2020. Quantitative assessment of the risk of airborne transmission of SARS-CoV-2 infection: prospective and retrospective applications. Environ. Int. 145, 106112 https://doi.org/10.1016/j.envint.2020.106112.

Chatoutsidou, S.E., Lazaridis, M., 2019. Assessment of the impact of particulate dry deposition on soiling of indoor cultural heritage objects found in churches and museums/libraries. J. Cult. Herit. 39, 221–228. https://doi.org/10.1016/j.culher.2019.02.017.

Chen, W., Zhang, N., Wei, J., Yen, H.-L., Li, Y., 2020. Short-range airborne route dominates exposure of respiratory infection during close contact. Build. Environ. 176, 106859 https://doi.org/10.1016/j.buildenv.2020.106859.

Cortellessa, G., Stabile, L., Arpino, F., Faleiros, D.E., van den Bos, W., Morawska, L., Buonanno, G., 2021. Close proximity risk assessment for SARS-CoV-2 infection. Sci. Total Environ. 794, 148749 https://doi.org/10.1016/j.scitotenv.2021.148749.

d'Ambrosio Alfano, F.R., Dell'Isola, M., Ficco, G., Tassini, F., 2012. Experimental analysis of air tightness in Mediterranean buildings using the fan pressurization method. Build. Environ. 53, 16–25. https://doi.org/10.1016/j.buildenv.2011.12.017.

Dbouk, T., Drikakis, D., 1994. On airborne virus transmission in elevators and confined spaces. Phys. Fluids 33 (2021). https://doi.org/10.1063/5.0038180.

Dbouk, T., Drikakis, D., 2020. On coughing and airborne droplet transmission to humans. Phys. Fluids 32, 053310. https://doi.org/10.1063/5.0011960.

Dbouk, T., Drikakis, D., 2020. Weather impact on airborne coronavirus survival. Phys. Fluids 32, 093312. https://doi.org/10.1063/5.0024272.

Duguid, J.P., 1945. The numbers and the sites of origin of the droplets expelled during expiratory activities. Edinb. Med. J. LII (II), 385–401.

Evans, M.J., 2020. Avoiding COVID-19: aerosol guidelines. MedRxiv. https://doi.org/10.1101/2020.05.21.20108894.

Fears, A.C., Klimstra, W.B., Duprex, P., Hartman, A., Weaver, S.C., Plante, K.C., Mirchandani, D., Plante, J.A., Aguilar, P.V., Fernández, D., Nalca, A., Totura, A., Dyer, D., Kearney, B., Lackemeyer, M., Bohannon, J.K., Johnson, R., Garry, R.F., Reed, D.S., Roy, C.J., 2020. Comparative dynamic aerosol efficiencies of three emergent coronaviruses and the unusual persistence of SARS-CoV-2 in aerosol suspensions. MedRxiv. https://doi.org/10.1101/2020.04.13.20063784.

Greenhalgh, T., Jimenez, J.L., Prather, K.A., Tufekci, Z., Fisman, D., Schooley, R., 2021. Ten scientific reasons in support of airborne transmission of SARS-CoV-2. Lancet 397, 1603–1605. https://doi.org/10.1016/S0140-6736(21)00869-2.

Hammersley, J.M., Handscomb, D.C., 1964. Monte Carlo Methods. Chapman and Hall, London & New York.

International Commission on Radiological Protection, 1994. Human respiratory tract model for radiological protection. A report of a Task Group of the International Commission on Radiological Protection. Ann. ICRP 24, 1–482. https://doi.org/10.1016/0146-6453(94)90029-9.

International Organization for Standardization, ISO/IEC 17043:2010 Conformity assessment - General requirements for proficiency testing, 2010.

International Organization for Standardization, ISO 15189:2012: Medical laboratories - Requirements for quality and competence, (2012).

International Organization for Standardization, ISO/IEC 17025:2017: General requirements for the competence of testing and calibration laboratories, (2017).

Johnson, G.R., Morawska, L., Ristovski, Z.D., Hargreaves, M., Mengersen, K., Chao, C.Y. H., Wan, M.P., Li, Y., Xie, X., Katoshevski, D., Corbett, S., 2011. Modality of human expired aerosol size distributions. J. Aerosol Sci. 42, 839–851. https://doi.org/10.1016/j.jaerosci.2011.07.009.

Joint Committee for Guides in Metrology, Evaluation of measurement data — Supplement 1 to the "Guide to the expression of uncertainty in measurement" - Propagation of distributions using a Monte Carlo method, 2008.

Joint Committee for Guides in Metrology, Evaluation of measurement data - Guide to the expression of uncertainty in measurement., 2008.

Lakey, P.S.J., Won, Y., Shaw, D., Østerstrøm, F.F., Mattila, J., Reidy, E., Bottorff, B., Rosales, C., Wang, C., Ampollini, L., Zhou, S., Novoselac, A., Kahan, T.F., DeCarlo, P. F., Abbatt, J.P.D., Stevens, P.S., Farmer, D.K., Carslaw, N., Rim, D., Shiraiwa, M., 2021. Spatial and temporal scales of variability for indoor air constituents. Commun. Chem. 4, 110. https://doi.org/10.1038/s42004-021-00548-5.

Lednicky, J.A., Lauzardo, M., Fan, Z.H., Jutla, A., Tilly, T.B., Gangwar, M., Usmani, M., Shankar, S.N., Mohamed, K., Eiguren-Fernandez, A., Stephenson, C.J., Alam, Md.M., Elbadry, M.A., Loeb, J.C., Subramaniam, K., Waltzek, T.B., Cherabuddi, K., Morris, J. G., Wu, C.-Y., 2020. Viable SARS-CoV-2 in the air of a hospital room with COVID-19 patients. Int. J. Infect. Dis. 100, 476–482. https://doi.org/10.1016/j.ijid.2020.09.025.

Li, Y., 2021. The respiratory infection inhalation route continuum. Indoor Air 31, 279–281. https://doi.org/10.1111/ina.12806.

Liu, Y., Ning, Z., Chen, Y., Guo, M., Liu, Y., Gali, N.K., Sun, L., Duan, Y., Cai, J., Westerdahl, D., Liu, X., Xu, K., Ho, K.-F., Kan, H., Fu, Q., Lan, K., 2020. Aerodynamic analysis of SARS-CoV-2 in two Wuhan hospitals. Nature 582, 557–560. https://doi.org/10.1038/s41586-020-2271-3.

Mikszewski, A., Stabile, L., Buonanno, G., Morawska, L., 2021. The airborne contagiousness of respiratory viruses: a comparative analysis and implications for mitigation. Geosci. Front., 101285 https://doi.org/10.1016/j.gsf.2021.101285.

Miller, S.L., Nazaroff, W.W., Jimenez, J.L., Boerstra, A., Buonanno, G., Dancer, S.J., Kurnitski, J., Marr, L.C., Morawska, L., Noakes, C., 2020. Transmission of SARS-CoV-2 by inhalation of respiratory aerosol in the Skagit Valley Chorale superspreading event. Indoor Air. https://doi.org/10.1111/ina.12751.

Morawska, L., Buonanno, G., 2021. The physics of particle formation and deposition during breathing. Nat. Rev. Phys. 3, 300–301. https://doi.org/10.1038/s42254-021-00307-4.

Morawska, L., Cao, J., 2020. Airborne transmission of SARS-CoV-2: the world should face the reality. Environ. Int. 139, 105730 https://doi.org/10.1016/j.envint.2020.105730.

Morawska, L., Johnson, G.R., Ristovski, Z.D., Hargreaves, M., Mengersen, K., Corbett, S., Chao, C.Y.H., Li, Y., Katoshevski, D., 2009. Size distribution and sites of origin of droplets expelled from the human respiratory tract during expiratory activities. J. Aerosol Sci. 40, 256–269. https://doi.org/10.1016/j.jaerosci.2008.11.002.

Morawska, L., Tang, J.W., Bahnfleth, W., Bluyssen, P.M., Boerstra, A., Buonanno, G., Cao, J., Dancer, S., Floto, A., Franchimon, F., Haworth, C., Hogeling, J., Isaxon, C., Jimenez, J.L., Kurnitski, J., Li, Y., Loomans, M., Marks, G., Marr, L.C., Mazzarella, L., Melikov, A.K., Miller, S., Milton, D.K., Nazaroff, W., Nielsen, P.V., Noakes, C., Peccia, J., Querol, X., Sekhar, C., Seppänen, O., Tanabe, S., Tellier, R., Tham, K.W., Wargocki, P., Wierzbicka, A., Yao, M., 2020. How can airborne transmission of COVID-19 indoors be minimised? Environ. Int. 142, 105832 https://doi.org/10.1016/j.envint.2020.105832.

Nissen, K., Krambrich, J., Akaberi, D., Hoffman, T., Ling, J., Lundkvist, Å., Svensson, L., Salaneck, E., 2020. Long-distance airborne dispersal of SARS-CoV-2 in COVID-19 wards. Sci. Rep. 10, 19589. https://doi.org/10.1038/s41598-020-76442-2.

Pan, Y., Zang, D., Yang, P., Poon, L.M., Wang, Q., 2020. Viral load of SARS-CoV-2 in clinical samples. Lancet 20, 411–412.

Randall, K., Ewing, T.E., Marr, L., Jimenez, J., Bourouiba, L., 2021. How did we get here: what are droplets and aerosols and how far do they go? a historical perspective on the transmission of respiratory infectious diseases. SSRN 11. ⟨https://ssrn.com/abstract=3829873⟩.

Regione Lazio, DCA 8/2011 - Requisiti minimi autorizzativi per l'esercizio delle attività sanitarie e socio-sanitarie, 2011.

Decreto del Presidente della Repubblica, Approvazione dell'atto di indirizzo e coordinamento alle regioni e alle province autonome di Trento e di Bolzano, in materia di requisiti strutturali, tecnologici ed organizzativi minimi per l'esercizio delle attività sanitarie da parte delle strutture pubbliche e private., 1997.

Robotto, A., Civra, A., Quaglino, P., Polato, D., Brizio, E., Lembo, D., 2021. SARS-CoV-2 airborne transmission: a validated sampling and analytical method. Environ. Res 200, 111783. https://doi.org/10.1016/j.envres.2021.111783.

Robotto, A., Quaglino, P., Lembo, D., Morello, M., Brizio, E., Bardi, L., Civra, A., 2021. SARS-CoV-2 and indoor/outdoor air samples: a methodological approach to have consistent and comparable results. Environ. Res 195, 110847. https://doi.org/10.1016/j.envres.2021.110847.

Robotto, A., Lembo, D., Quaglino, P., Brizio, E., Polato, D., Civra, A., Cusato, J., Di Perri, G., 2022. Wastewater-based SARS-CoV-2 environmental monitoring for Piedmont, Italy. Environ. Res 203, 111901. https://doi.org/10.1016/j.envres.2021.111901.

Rudnick, S.N., Milton, D.K., 2003. Risk of indoor airborne infection transmission estimated from carbon dioxide concentration. Indoor Air 13, 237–245. https://doi.org/10.1034/j.1600-0668.2003.00189.x.

Rudnick, S.N., Milton, D.K., 2003. Risk of indoor airborne infection transmission estimated from carbon dioxide concentration. Indoor Air 13, 237–245. https://doi.org/10.1034/j.1600-0668.2003.00189.x.

Santarpia, J.L., Rivera, D.N., Herrera, V.L., Morwitzer, M.J., Creager, H.M., Santarpia, G. W., Crown, K.K., Brett-Major, D.M., Schnaubelt, E.R., Broadhurst, M.J., Lawler St, J. V., Reid, P., Lowe, J.J., 2020. Aerosol and surface contamination of SARS-CoV-2 observed in quarantine and isolation care. Sci. Rep. 10, 12732. https://doi.org/10.1038/s41598-020-69286-3.

Stabile, L., Pacitto, A., Mikszewski, A., Morawska, L., Buonanno, G., 2021. Ventilation procedures to minimize the airborne transmission of viruses in classrooms. Build. Environ. 202, 108042 https://doi.org/10.1016/j.buildenv.2021.108042.

Stadnytskyi, V., Bax, C.E., Bax, A., Anfinrud, P., 2020. The airborne lifetime of small speech droplets and their potential importance in SARS-CoV-2 transmission. Proc. Natl. Acad. Sci. USA 117, 11875–11877. https://doi.org/10.1073/pnas.2006874117.

Stern, R.A., Koutrakis, P., Martins, M.A.G., Lemos, B., Dowd, S.E., Sunderland, E.M., Garshick, E., 2021. Characterization of hospital airborne SARS-CoV-2. Respir. Res. 22, 73. https://doi.org/10.1186/s12931-021-01637-8.

Sze, G.N., Chao, C.Y.H., 2010. Review and comparison between the Wells–Riley and dose-response approaches to risk assessment of infectious respiratory diseases. Indoor Air 20, 2–16. https://doi.org/10.1111/j.1600-0668.2009.00621.x.

van Doremalen, N., Bushmaker, T., Morris, D.H., Holbrook, M.G., Gamble, A., Williamson, B.N., Tamin, A., Harcourt, J.L., Thornburg, N.J., Gerber, S.I., Lloyd-Smith, J.O., de Wit, E., Munster, V.J., 2020. Aerosol and surface stability of SARS-CoV-2 as compared with SARS-CoV-1. New Engl. J. Med. 382, 1564–1567. https://doi.org/10.1056/NEJMc2004973.

Wagner, B.G., Coburn, B.J., Blower, S., 2009. Calculating the potential for within-flight transmission of influenza A (H1N1). BMC Med. 7, 81. https://doi.org/10.1186/1741-7015-7-81.

Wagner, B.G., Coburn, B.J., Blower, S., 2009. Calculating the potential for within-flight transmission of influenza A (H1N1). BMC Med. 7, 81. https://doi.org/10.1186/1741-7015-7-81.

Yang, W., Marr, L.C., 2011. Dynamics of airborne influenza a viruses indoors and dependence on humidity. PLOS ONE 6, e21481. https://doi.org/10.1371/journal.pone.0021481.